NUCL SCI TECH (2016) 27:1
DOI 10.1007/s41365-016-0013-x

Characterization of crud deposited on fuel rods under HWC environment in Kuosheng Nuclear Power Plant

Tsuey-Lin Tsai[1] · **Te-Yen Su**[1] · **Tsung-Yuan Wang**[1] · **Tsen-Yu Yang**[1]

Received: 24 May 2015 / Revised: 17 July 2015 / Accepted: 18 July 2015 / Published online: 27 February 2016

Abstract Under normal water chemistry conditions, the oxygen and hydrogen peroxide produced by water radiolysis in the coolant of boiling water reactors (BWRs) can lead to intergranular stress corrosion cracking in the constituent materials of plant components. This fact has led to the wide-scale adoption of hydrogen water chemistry (HWC) in the nuclear industry to counteract these effects. This study seeks to characterize the metallic composition and the surface properties of the constituent materials of plant components in order to determine their effects on the accumulation of chalk river unidentified deposits (crud) on fuel rods in the BWR Unit-1 of the Kuosheng Nuclear Power Plant in Taiwan. Inductively coupled plasma-atomic emission spectroscopy was used to calculate the concentrations of surface crud and gamma spectrometry was used to determine the radioactivity of the corrosion products, as well as their axial distribution across the surface of the fuel rods. X-ray diffraction analysis and scanning electron microscopy/energy-dispersive X-ray spectroscopy were used to identify the crystalline phase and morphology of the crud as irregular shapes and flakes. The amount of crud deposited during the fourth fuel cycle exceeded that of the third fuel cycle due to extended burn-up time. Our analytical results indicate that the implementation of HWC had no significant effect on the characteristics of subsequent crud.

Keywords Crud · Hydrogen water chemistry (HWC) · Normal water chemistry (NWC) · Fuel rod

1 Introduction

High-purity water is used for the neutron moderator and primary coolant in the boiling water reactors (BWRs). However, the radiolysis of water inevitably leads to the accumulation of oxidants in the reactor coolant. Under normal water chemistry (NWC) conditions, the concentration of total oxidants ($O_2 + H_2O_2$) can reach 200 ppb (as measured in the recirculation system), which is sufficient to produce intergranular stress corrosion cracking (IGSCC) in the Ni-base alloys and stainless steel in the core components. The recombination of O_2 with H_2 causes a gradual decrease in the concentration of O_2 in the recirculation system. Thus, H_2 is injected into the reactor feed water to mitigate the effects of oxidation, thereby reducing the initiation and propagation of cracks in the piping and internal components of the reactor. The first, full-time implementation of hydrogen water chemistry (HWC) was demonstrated at the U.S Dresden-2 BWR in 1982 [1], and since that time, HWC technology has been the subject of extensive research [2–4]. Hydrogen is among the most effective additives for the reduction of oxygen. It is also non-corrosive and non-toxic and does not alter the pH of the system [5]. However, the addition of large quantities of H_2 can lead to two problems: (a) increased radiation levels in the main steam lines and turbines resulting from the formation of volatile chemical species: ^{16}N, via a (n, p) reaction with ^{16}O under reducing conditions [6]; and (b) an increase in drywell dose rates resulting from the transport

✉ Tsuey-Lin Tsai
polly@iner.gov.tw

[1] Chemistry Division, Institute of Nuclear Energy Research, Longtan, Taoyuan, Taipei

of ^{60}Co in fuel corrosion products, which are subsequently deposited on the surfaces of out-of-core materials.

The term crud refers to corrosion products from structural materials or internal reactor components, which are introduced into the core of a reactor following fuel-rod failure or cladding breaches [7, 8]. The crud in nuclear power plants is also referred to as iron crud [9], due to the fact that nuclear power plants are composed mainly of iron. Large quantities of crud in the BWR coolant can increase the amount of radiation exposure to which workers are exposed, particularly following the buildup of ^{60}Co [2, 10]. Crud vary according to the type of reactor and fuel assembly.

Since 2006, HWC has been introduced at two BWRs in Taiwan. This study used the characterization of crud and analytical results related to its composition and morphology as baseline reference values with which to guide the transition from NWC to HWC. The first two campaigns, KS1-EX1 and KS1-EX3, under NWC conditions were conducted during the outage of end of cycle (EOC) 15 in September 2001 and during the outage of EOC 16 in January 2003, respectively, by the lead used assembly (LUA) surveillance program prior to the addition of hydrogen. The initial hydrogen concentration in this nuclear power plant was 0.5 ppm in November 2006 (6 months after the beginning of cycle 19), which increased to 1 ppm in June 2009 (2 months after the beginning of cycle 21) [11].

As shown in Table 1, the two fuel assemblies (K1D015 and K1D059) were in operation for three fuel cycles under HWC conditions. This resulted in an average assembly burn-up of approximately 45.9 GWd/MTU and 43.7 GWd/MTU for K1D015 and K1D059, respectively. Crud were scraped from both assemblies during the outage of cycle 21 in October 2010 [11], and examinations were scheduled after cycle 22. However, limitations in the available withdraw force were encountered while attempting the removal of channel assemblies during the examinations of K1D015 (burn-up of 50.6 GWd/MTU) and K1D059 (burn-up of 49.4 GWd/MTU). The high burn-up (~50 GWd/MTU) in these two assemblies may have contributed to the high fractional forces between the spacer and channel [12]. Thus, we selected the other two fuel bundles (with burn-ups of 42.6 GWd/MTU and 46.3 GWd/MTU for K1D085 and K1D131, respectively) for crud analysis following the outage of cycle 22. This paper presents the results obtained from the analysis of crud collected from fuel rods during and after refueling outages.

2 Experimental

2.1 Crud scraping

In this study, a single stroke of a scraper with an area of about 2 cm^2 on the fuel rods was used to define the sampling area. Crud was removed using a stream of water, which was then passed through a vacuum filter (0.45 µm pore size) for sample collection. Crud samples were scraped at 5 mid-span axial locations (spans 1–5) on two rods located on different sides (A5 and L5) of each assembly, while held underwater in the spent fuel storage pool. The spacer numbering and span elevations of the ATRIUM-10 fuel assembly for the sampling locations are presented in Fig. 1. The locations on the rods from which crud samples were obtained are presented in Fig. 2. All samples were loaded into casks for shipment to laboratories at the Institute of Nuclear Energy Research (INER) for further analysis.

2.2 Sample pretreatment

X-ray diffraction (XRD) and scanning electron microscopy (SEM) measurements were performed on small samples cut from the filter paper. Chemical and radiochemical analysis of the crud using inductively coupled plasma-atomic emission spectroscopy (ICP-AES) and gamma spectrometry required pretreatment using wet oxidation and the total dissolution of the filtered samples. The samples were completely dissolved in a solution of concentrated HNO_3 (69 %) and HCl (37 %) (1:1). Following the addition of several drops of H_2O_2 (30 %) to destroy any

Table 1 Burn-up and core location information of the examined fuel assemblies

Assembly	HWC operation	Program name Crud sampling time	EOC-19 Core location	EOC-20 Core location	EOC-21 Core location	EOC-21 Burn-up[a]	EOC-22 Core location	EOC-22 Burn-up
K1D015	Cycle 21	KS1-EX5	35–42	43–46	33–38	45.9	45–50	50.6
K1D059	(2009.04.12–2010.10.06)	(2010.10.11–2010.10.19)	9–30	5–36	15–46	43.7	03–38	49.4
K1D085	Cycle 22	KS1-EX6	45–26	49–16	49–16	38.4	31–02	42.6
K1D131	(2010.10.31–2012.03.11)	(2012.06.14–2012.06.26)	23–30	27–06	07–18	41.6	07–12	46.3

[a] Burn-up unit: GWd/MTU

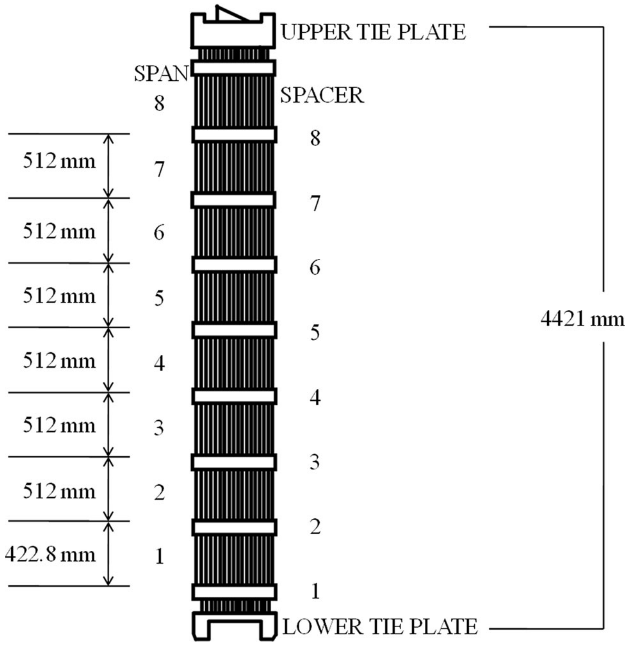

Fig. 1 Dimensions and span elevations of the fuel assembly

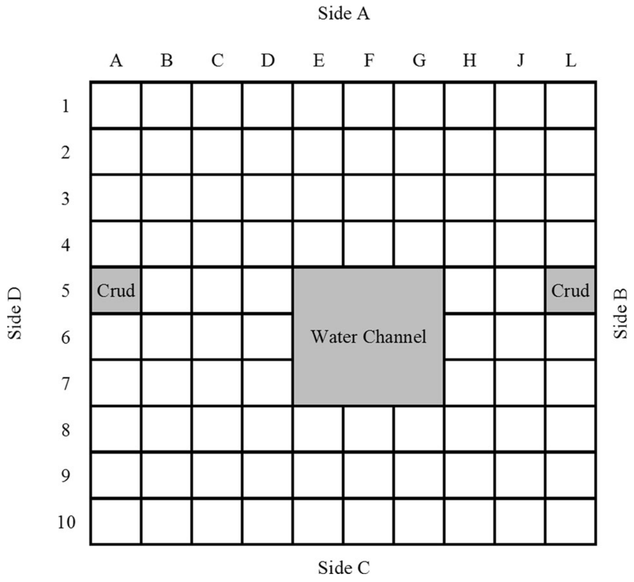

Fig. 2 Location of crud sampling on used rods

remaining organic substances, the samples were evaporated to near-dryness in Teflon containers on a hot plate. Finally, the samples were diluted in DIW (100 ml) in a volumetric flask for quantitative analysis.

2.3 SEM/EDS

The topography of the samples was analyzed using a scanning electron microscope with an integrated energy-dispersive X-ray analysis system (JEOL, JSM-6510) at high resolution (3.0 nm at 30 kV). After drying under an infrared lamp (250 W) for approximately 1 h, the voltage was set to 20 kV and images taken at an appropriate magnification ratio were selected.

2.4 XRD

The analysis of crud samples was performed using a Bruker D8 Advance diffractometer operated at 40 kV and 40 mA in a ceramic Cu X-ray (1.5418 Å) tube. Scanning was performed in the range of 20°–60° (2θ) at a speed of 1°/min. A LynxEYE compound silicon strip detector with lower background counts (<0.1 cps) was employed. Diffraction spectra of the sample and references were analyzed using TOPAS Spectra software to calculate the crystal content of the samples.

2.5 ICP-AES

The following major elements were detected using ICP-AES analysis (Horiba JY Ultima 2): Fe, Co, Cu, Ni, Cr, Zn, and Mn.

2.6 Gamma spectrometer

Activity concentrations in the crud samples were obtained using a high-purity Ge-detector (HPGe; Canberra GC 4020) with a 1024 multi-channel analyzer (Canberra DSP 9660). The activity concentrations of ^{54}Mn, ^{60}Co, ^{58}Co, and ^{59}Fe were calculated according to the gamma spectra using Canberra Genie 2000 software.

3 Results and discussion

3.1 Elemental composition and activity concentration of deposits

During the operation of the plant, impurities accumulate in the reactor water due to the ingress of soluble and insoluble metallic species through the feed water system. Table 2 lists the average concentrations of metallic species (as determined by ICP-AES) in the reactor water and feed water. The most common impurity is iron and the minor impurities include copper, zinc, and nickel, which accumulate in the form of crud on the surfaces of fuel cladding and can be viewed as a product of the boiling that occurs in the core. Table 3 lists the average metallic compositions and activity concentrations of corrosion products accumulated on the surface of fuel rods. More than 97.0 wt% of the content is made up of iron, with other elements accounting for <3.0 wt%. The Fe can be traced to carbon steel, stainless steel, and other iron-based alloys. After Fe, the

Table 2 Concentrations of metallic species in reactor water (A) and feed water (B) (mean values for EOC21 and EOC22), *W* represents the weight of the composition

Metallic species	Average concentration							
	Insoluble (A)		Soluble (A)		Insoluble (B)		Soluble (B)	
	C (ppb)	*W*(wt%)	*C* (ppb)	*W* (wt%)	*C* (ppb)	*W* (wt%)	*C* (ppb)	*W* (wt%)
Fe	1.92	57.42	1.22	30.73	0.705	97.44	0.010	13.10
Cu	0.49	14.69	1.40	35.14	0.007	0.90	0.040	55.17
Ni	0.19	5.55	0.24	5.92	0.002	0.21	0.013	17.93
Zn	0.54	16.04	0.90	22.67	0.003	0.35	0.003	3.45
Cr	0.21	6.30	0.22	5.54	0.004	0.48	0.004	5.52
Co					0.005	0.62	0.004	4.83

Table 3 Average element composition and activity concentrations of crud deposited on fuel rods

Fuel assembly	Fuel rod	Elemental compositions ($\mu g/cm^2$)							Activity concentrations (MBq/cm^2)			
		Cr	Mn	Fe	Co	Ni	Cu	Zn	^{54}Mn	^{58}Co	^{59}Fe	^{60}Co
K1D015	A5	0.318	0.712	268.3	0.231	1.195	4.008	0.240	0.504	0.021	0.142	0.268
K1D059		0.141	0.533	152.0	0.179	0.714	2.865	0.193	0.307	0.015	0.087	0.165
K1D085		1.061	3.026	1228	0.653	6.256	3.312	0.707	0.774	0.013	0.045	1.013
K1D131		1.265	3.348	1313	0.793	7.070	8.075	0.635	1.100	0.021	0.069	1.249
K1D015	L5	0.235	0.582	206.0	0.198	1.086	3.629	0.537	0.416	0.020	0.124	0.233
K1D059		0.271	0.807	305.2	0.231	1.353	4.958	0.323	0.520	0.021	0.152	0.306
K1D085		0.850	1.732	698.4	0.271	3.274	1.838	0.575	0.413	0.007	0.033	0.354
K1D131		1.013	2.750	1121	0.605	5.856	3.165	0.564	0.677	0.011	0.058	1.135

most common elements in the crud are Ni and Cu, which can be attributed to the use of a copper–nickel condenser tube at this plant. Ni and Cr can also be traced back to the stainless steel and Inconel, whereas the Cu mostly leaches from copper-based alloys. Mn is common in stainless steel and carbon steel. The Co content in the crud is very low; however, it is an important source of the activated product ^{60}Co. The average element compositions during the refueling outages of EOC 15 (fuel cycle 3) and EOC 16 (fuel cycle 4) under NWC conditions are consistent with the results obtained after the implementation of HWC [13].

The main nuclides included the following activated corrosion products: ^{54}Mn, ^{59}Fe, ^{60}Co, and ^{58}Co. The axial concentration distributions of Fe with ^{54}Mn and ^{59}Fe activities, Ni with ^{58}Co activities, and Co with ^{60}Co activities in the crud are presented in Figs. 3, 4, and 5. Similar trends can be observed in the two groups of analytical results for the EOC 21 (K1D015 and K1D059) and EOC 22 (K1D085 and K1D131) crud samples. The activity of radionuclides in the adherent oxide layer is proportional to that of the crud deposited on the fuel rods. The distribution patterns of ^{54}Mn and ^{59}Fe in Fig. 3b, c are similar to those in Fig. 3a. This is not unexpected, due to the fact that ^{54}Fe and ^{58}Fe are the mother isotopes of ^{54}Mn and ^{59}Fe via the activation reactions of [^{54}Fe(n, p)^{54}Mn] and [^{58}Fe(n, γ)^{59}Fe], respectively. Furthermore, ^{54}Mn and ^{59}Fe exist for only a short period following the shutdown of the reactor due to their short half-lives. As shown in Fig. 4a, b, the axial distribution of ^{58}Co was similar to that of Ni. ^{58}Co is the daughter isotope of ^{58}Ni (natural isotope; 68.08 % abundance), formed through the activation [^{58}Ni(n, p)^{58}Co] of nickel from stainless steel and nickel-based alloys. Similarly, the distribution pattern of ^{60}Co, as obtained by neutron irradiation [^{59}Co(n, γ)^{60}Co], is similar to that observed in Co, as shown in Fig. 5a, b. A greater amount of crud was deposited on spans 1–2 (at a height of 50–100 cm from the bottom) than on spans 3–5 (at a height of 00–250 cm from the bottom) of the rods. Spans 1–2 (where the boiling starts) were fully immersed in the water phase and thus had a higher probability of deposition, whereas spans 3–5 are in the upper part of the core close to the steam phase [13], where deposition is less likely to occur.

The axial profiles of the massic and activity concentrations of EOC 15-KBE 301 (fuel cycle 3) and KBE 302-EOC 16 (fuel cycle 4) under NWC conditions are consistent with the results obtained following the implementation of HWC [13]. We also analyzed a large number of L5 fuel deposit samples. The results of the concentration and activity distributions along the length of the fuel rods present trends similar to those obtained from the A5 crud

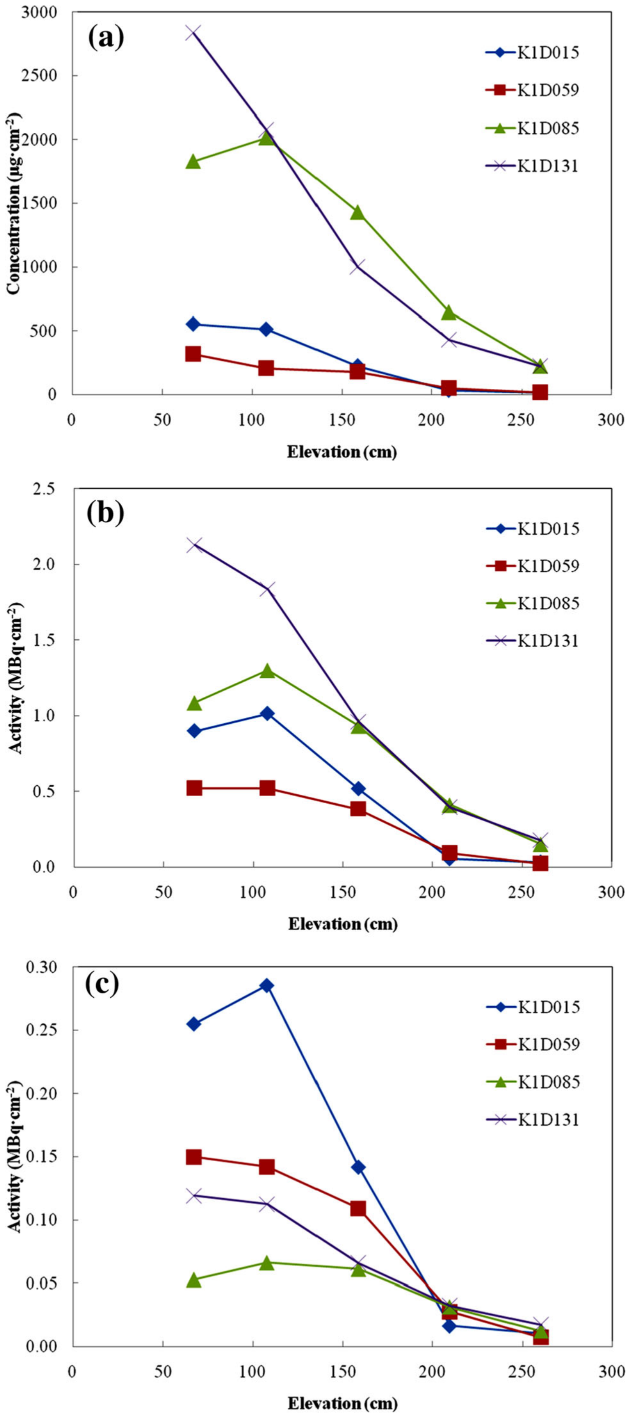

Fig. 3 (Color online) Axial profiles of A5 crud samples collected in 2010 and 2012: (**a**) Fe; (**b**) ^{54}Mn; and (**c**) ^{59}Fe

samples [12, 15]. Lin [14] claimed that the amount of fuel surface deposit and its chemical composition depend on the corrosion product input from the condensate and feed water systems.

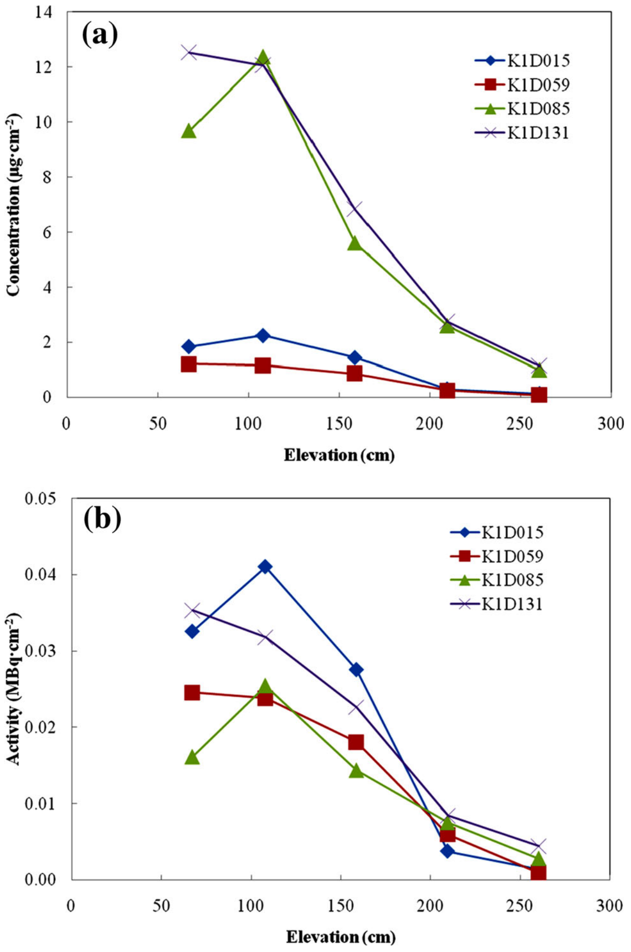

Fig. 4 (Color online) Axial profiles of A5 crud samples collected in 2010 and 2012: (**a**) Ni; and (**b**) ^{58}Co

3.2 Interpretation of ^{58}Co/^{60}Co ratios in the crud samples

Figure 6 presents the activity ratios of ^{58}Co/^{60}Co in the crud samples. K1D015 and K1D059 were collected at EOC 21 (3rd burn-up) in 2010; K1D085 and 131 were obtained at EOC 22 (4th burn-up) in 2012. Jung et al. [16] suggested that similarities in the values of radioactivity ratios of ^{58}Co to ^{60}Co were an indication of fuels with a similar burn-up history in the reactor core. The average radioactivity ratios of ^{58}Co/^{60}Co in the fuel assemblies of K1D085 and K1D131 are considerably lower than those of K1D015 and K1D059. This can be partly explained by the fact that the former remained in the spent fuel pool for a longer duration than did the latter. It can also be attributed to the considerable difference in the half-lives of the two radionuclides (i.e., 70.8 days for ^{58}Co and 5.27 years for ^{60}Co). Thus, the radioactivity ratio could be used to determine how long the crud was present in the reactor core.

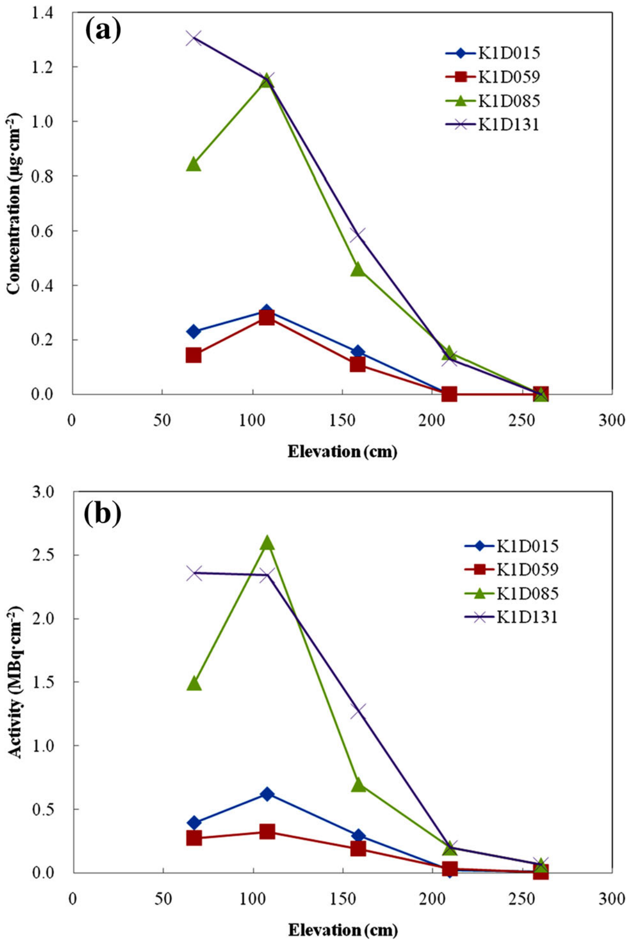

Fig. 5 (Color online) Axial profiles of A5 crud samples collected in 2010 and 2012: (**a**) Co; and (**b**) ^{60}Co

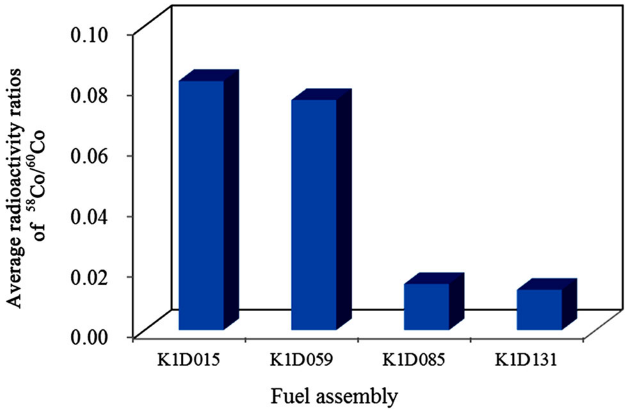

Fig. 6 (Color online) Radioactivity ratios of ^{58}Co/^{60}Co in crud samples

3.3 SEM and XRD analysis

Figure 7a–d presents SEM images showing the morphology of crud on the fuel rods. Most of the corrosion

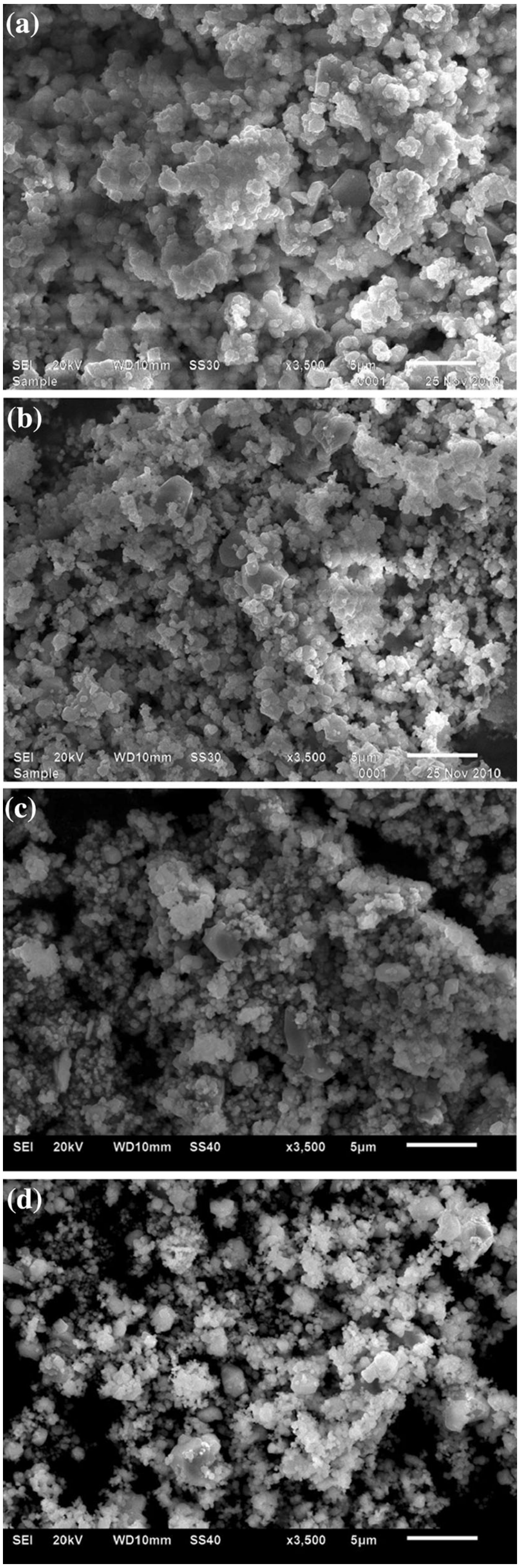

Fig. 7 SEM photographs of crud samples: (**a**) KID015 L5 span 5; (**b**) KID059 L5 span 2; (**c**) K1D085 A5 span 5; (**d**) K1D131 A5 span 4

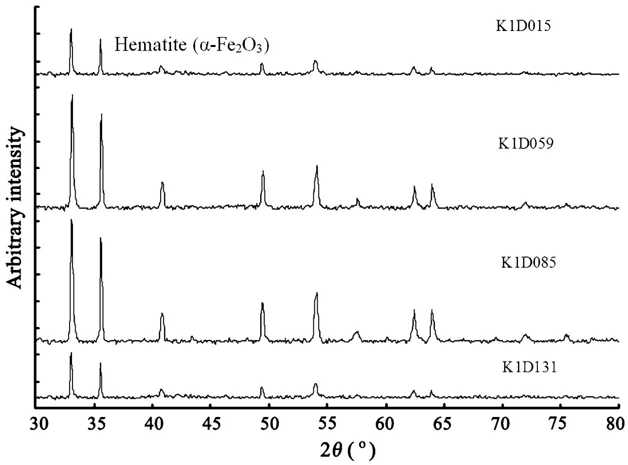

Fig. 8 X-ray diffraction patterns of crud on fuel rods of four fuel assemblies

products display clusters of irregularly shaped smaller (0.1–0.3 μm) or larger (0.5–2.0 μm) particles in the sub-micron range. A small number of the samples contained visible "flakes" within the crud. These flakes were defined as fragments of crud with the largest dimension greater than or equal to 5 μm. Orlov et al. identified several types of cubic clusters as spinel crystal structures [17]. The constituent materials may include trace quantities of franklinite ($ZnFe_2O_4$), trevorite ($NiFe_2O_4$), and jacobsite ($MnFe_2O_4$). EDS analysis identified cubic spinel-type crystals of $MnFe_2O_4$ with a stoichiometric Mn/Fe ratio of 1:2.

Crud samples were scanned using XRD and analyzed with TOPAS to characterize the crystal content. As shown in Fig. 8, reddish α-Fe_2O_3 (hematite) was the primary form of iron in the loosely adhered outer layer of the BWR fuel rods. XRD analysis of the crud gave no indication that they contain Fe_3O_4, which could theoretically change into Fe_3O_4 if hydrogen were used as a reductant. Nevertheless, this reaction would require very high temperatures ($\sim$600 °C) [18]. These results corroborate the supposition that the transition of α-Fe_2O_3 to Fe_3O_4 was kinetically inhibited at temperatures of only 288 °C. Under HWC conditions, the results obtained in the fourth fuel cycle were the same as those obtained in the third [15]. In the report by Liang and Chien, hematite was the major constituent deposited on the fuel rods in an NWC environment, accounting for more than 95 wt% of the total [13]. The crud samples in the report by Judd et al. included almost 100 % α-Fe_2O_3 with no detectable Fe_3O_4 type under HWC. They reported no adverse transitional effects associated with bundles that were exposed to NWC, as well as HWC [19]. Beverskog and Puigdomenech stated that the nature of the crud depended on the Ni/Fe ratios at 285 °C; i.e., both $NiFe_2O_4$ and α-Fe_2O_3 can form when Ni/Fe is <0.5 [20]. In this study, the Ni/Fe ratio observed in the four fuel assemblies was in the range of only 0.005. These negligible quantities of Ni resulted in the formation of α-Fe_2O_3 as the preferred phase.

4 Conclusion

The main concluding remarks of this study are as follows:

(1) The order of abundance (Fe > Cu > Ni) of the major constituents of the crud in this study did not change following the implementation of HWC, and the minor elements (Mn, Co, Cr, and Zn) accounted for less than 0.5 % of the total material.

(2) The quantity of deposited crud on two of the fuel assemblies (K1D085 and K1D131) was far greater at EOC 22 than at EOC 21, due to a longer burn-up time in the reactor. In addition, the radioactivity ratio of ^{58}Co to ^{60}Co was lower at EOC 22 than at EOC 21, due to an extended storage period in the spent fuel pool.

(3) According to SEM/EDS data and XRD analysis, the particles of iron oxide varied widely in size from sub-μm to 5 μm and very small quantities of jacobsite were also observed. These results suggest that the crud are composed primarily of loosely adhered oxides with minor quantities of tenacious oxides.

(4) The implementation of HWC at the Kuosheng BWR plant did not promote the formation of iron compounds with a lower oxidation state (such as spinel-type Fe_3O_4). According to the XRD analytical results, after three or four fuel cycles, the predominant iron compound in the crud was fully oxidized α-Fe_2O_3.

(5) There is no indication that three or four cycles of HWC at this BWR plant had a significant effect on the characteristics of the subsequent deposition of crud.

Acknowledgments We wish to express our sincere gratitude to Mr. CHUNG Tsang-Hsien of the Radiochemistry Subsection of the Second Nuclear Power Plant of Taiwan Power Company for providing recent plant-related data. We also gratefully acknowledge Ms. CHIU Wan-June of the Institute of Nuclear Energy Research for providing technical information and valuable suggestions.

References

1. Y. Wada, S. Uchida, M. Nakamura et al., Empirical understanding of the dependency of hydrogen water chemistry

effectiveness on BWR designs. J. Nucl. Sci. Technol. **36**, 169–178 (1999). doi:10.1080/18811248.1999.9726195

2. C.C. Lin, F.R. Smith, R.L. Cowan, Effects of hydrogen water chemistry on radiation field buildup in BWRs. Nucl. Eng. Des. **166**, 31–36 (1996). doi:10.1016/0029-5493(96)01196-X
3. C.C. Lin , Hydrogen water chemistry technology in boiling water reactors. Nucl. Technol. **130**: 59–70 (2000) http://www.ans.org/store/article-3077/
4. H. Takiguchi, M. Sekiguchi, A. ABE et al., Evaluation of effectiveness of hydrogen water chemistry for different types of boiling water reactors. J. Nucl. Sci. Technol. **36**, 179–188 (1999). doi:10.1080/18811248.1999.9726196
5. T.K. Yeh, M.Y. Wang, The impact of power uprate on the corrosion mitigation effectiveness of hydrogen water chemistry in boiling water reactors. Nucl. Sci. Eng. **160**, 98–107 (2008). doi:10.13182/NSE07-38
6. C.C. Lin, Chemical behavior and steam transport of nitrogen-13 in BWR primary system. J. Radioanal. Nucl. Chem. **130**, 129–139 (1989). doi:10.1007/BF02037707
7. A. Orlov, C. Degueldre, H. Wiese et al., Corrosion product deposits on boiling-water reactor cladding: experimental and theoretical investigation of magnetic properties. J. Nucl. Mater. **416**, 117–124 (2011). doi:10.1016/j.jnucmat.2010.12.033
8. D.E. Janney, D.L. Porter, Characterization of phases in 'crud' from boiling-water reactors by transmission electron microscopy. J. Nucl. Mater. **362**, 104–115 (2007). doi:10.1016/j.jnucmat.2006.11.009
9. K. Ishigure, K. ABE, N. Nakajima et al., Water chemistry experience of nuclear power plants in Japan. J. Nucl. Sci. Technol. **26**, 145–156 (1989). doi:10.3327/jnst.26.145
10. C.C. Lin, A review of corrosion product transport and radiation field buildup in boiling water reactors. Prog. Nucl. Energy **51**, 207–224 (2009). doi:10.1016/j.pnucene.2008.05.005
11. T.L. Tsai, T.Y. Lin, T.Y. Su et al., Identification of chemical composition of CRUD depositing on fuel surface of a boiling water reactor (BWR-6) plant. Energy Proc. **14**, 867–872 (2012). doi:10.1016/j.egypro.2011.12.1025
12. T.L. Tsai, T.Y. Lin, T.Y. Su et al., Characterization of corrosion products deposited on fuel rods in a boiling water reactor (BWR-6) plant using hydrogen water chemistry (HWC). J. Radioanal. Nucl. Chem. **298**, 1235–1244 (2013). doi:10.1007/s10967-013-2489-8
13. C.H. Liang, C.C. Chien, Study of deposited crud composition on fuel surface of a boiling water reactor plant. in *Symposium on Water Chemistry and Corrosion of Nuclear Power Plants in Asia, Korea Atomic Energy Research Institute. Gyeongju, Korea, Oct. 11–13* (2005), pp. 196–201
14. C.C. Lin, *Radiochemistry in Nuclear Power Reactors* (National Academies Press, Washington, 1996), p. 4
15. T.L. Tsai, T.Y. Lin, T.Y. Su et al., Chemical and radiochemical analysis of corrosion products on BWR fuel surfaces. J. Radioanal. Nucl. Chem. **295**, 289–296 (2013). doi:10.1007/s10967-012-1864-1
16. S.H. Jung, K.J. Daub, J.W. Yeon et al., Investigation on exceptional fuel CRUD samples by using radioactivity ratios of cobalt isotopes. Appl. Radiat. Isot. **81**, 307–309 (2013). doi:10.1016/j.apradiso.2013.03.062
17. A.V. Orlov, R. Restani, G. Kuri et al., Investigation on a corrosion product deposit layer on a boiling water reactor fuel cladding. Nucl. Instrum. Methods B **268**, 297–305 (2010). doi:10.1016/j.nimb.2009.09.007
18. R.P. Viswanath, B. Viswanathan, M.V.C. Sastri, Kinetics of reduction of Fe_2O_3 to Fe_3O_4 by the constant temperature differential thermal analysis method. Thermochim. Acta **16**, 240–244 (1976). doi:10.1016/0040-6031(76)85063-0
19. B. Cheng, Hydrogen water chemistry fuel surveillance at Dresden-2.GE Nuclear Energy, Vallecitos Nuclear Center, Pleasanton, California, NP-6956-D, August 1990. http://www.epri.com/abstracts/Pages/ProductAbstract.aspx?ProductId=NP-6956-D
20. B. Beverskog, I. Puigdomenech, Solubility of fuel crud in BWR. in *Proceedings of water chemistry of nuclear reactor system 7* (British Nuclear Energy Society, London, 1996), pp. 144–149